DESIGNING TRANSCRANIAL MAGNETIC STIMULATION SYSTEMS

By:

K.R. Davey
M. Riehl

IEEE Transactions on Magnetics, vol.41, no.3, March 2005, pp. 1142-1149
Mark Riehl: Neuronetics, Inc.

PR - 374

Center for Electromechanics
The University of Texas at Austin
PRC, Mail Code R7000
Austin, TX 78712
(512) 471-4496

March 16, 2004

IEEE Trans on Magnetics

Designing Transcranial Magnetic Stimulation Systems

Kent Davey[1], Charles M. Epstein[2], and Mark Riehl[3]
[1]Center for Electromechanics, University of Texas, EME 133, Austin, TX 78758
[2] Neurology, Emory University, 1354 Clifton Clinic, Atlanta, GA 30322
[3] Neuronetics, Inc., One Great Valley Parkway - Suite 2, Malvern, PA 19355
March 16, 2004

Abstract

The process of designing optimized transcranial magnetic stimulation systems is explained. A method is outlined for identifying optimal system parameters such as the number of turns, the capacitor size, the working voltage, and the size of the stimulation coil. It is achieved by combining field analysis, linear and nonlinear circuit analysis, and neural strength – duration response parameters. Boundary element analysis is used to predict the electric field as a function of depth, frequency, current, and excitation coil size. The field analysis can be used to determine the inductance as a function of size, and in general current when a saturable core is used. Circuit analysis allows these electric field computations to be indexed against system parameters, and optimized for total system energy and stimulation coil size. System optimizations are dependent on desired stimulation depth. Among the distinguishing features of this work is the inherent treatment of excitation frequency as an unknown to be determined from optimization.

Introduction

The usefulness of magnetic field stimulation devices for the stimulation of neurons is well established, and considerable research has been directed to identifying appropriate coil shapes and efficiencies to minimize stimulation energy. After testing over 16,000 coil designs, Durand concludes that a clover leaf design is optimal for infinitely long fibers, whereas a butterfly coil is preferred for bent fibers [1]. Ravazzani gives attention to the skin and proximity effect losses within air coil systems, and recommends large diameter small cross-section coils to mitigate these losses [2]. Onuki performs an optimization to increase induced E using a three coil setup [3]. A genetic algorithm is employed to change the shape of the coils to maximize the induced field. The pulse width was selected a priori. Many papers have examined unusual coil designs to enhance focality [4][5]. This paper outlines a method for optimizing the stimulator system including the stimulator unit.

Among the principle contributions of this paper is the point that this frequency is intimitaely linked to the stimulation efficiency. It must be treated as an unknown.

Analysis Approach

The cortex is characterized by neural bends and terminations, both of which activate on the electric field, not its gradient. Because of the small conductivity of the cortex, the induced B field is considerably smaller than the source field. For air core stimulators, the magnetic field is dictated entirely by the source current $\vec{J}_s$. With time harmonic stimulation at frequency ω, the electric field is determined by combining Ampere's law and Faraday's law,

$$\nabla\times\nabla\times\vec{E} = j\omega\mu_0\vec{J}_s \qquad (1)$$

The electric field boundary condition $\hat{n} \cdot \vec{E} = 0$ must be imposed to insure no normal component current exists at the skull interface.
Fig. 1 shows a typical stimulation circuit in which low voltage ac is transformed to a higher voltage and then rectified. This higher voltage dc charges a capacitor which is fired via a thyristor switch into the stimulator core.

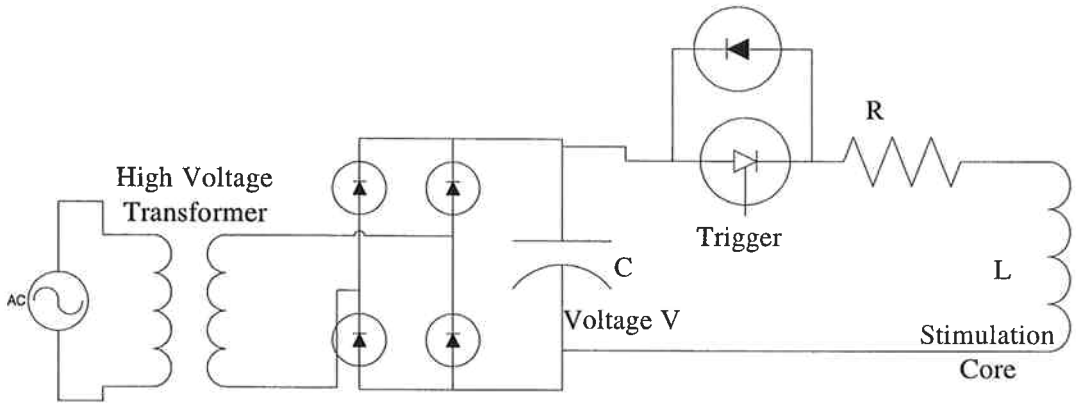

Fig. 1 Typical stimulation circuit.

This circuit goes through one complete resonance cycle before the diode thyristor shuts down and further current flow is prohibited by the diode. During the firing cycle, the circuit can be treated as a simple RLC resonance circuit. The current is

$$I(t) = \frac{V}{\omega L} e^{-(\alpha t)} \sin(\omega t),$$

where

$$\alpha = \frac{R}{2L} \qquad (2)$$

$$\omega = \sqrt{\frac{1}{LC} - \alpha^2}$$

This is the equation for a damped sinusoid. A typical trace with V=1.5 kV, C=15 μF, L=11 μH, and R=0.2 Ω is shown in Fig. 2.

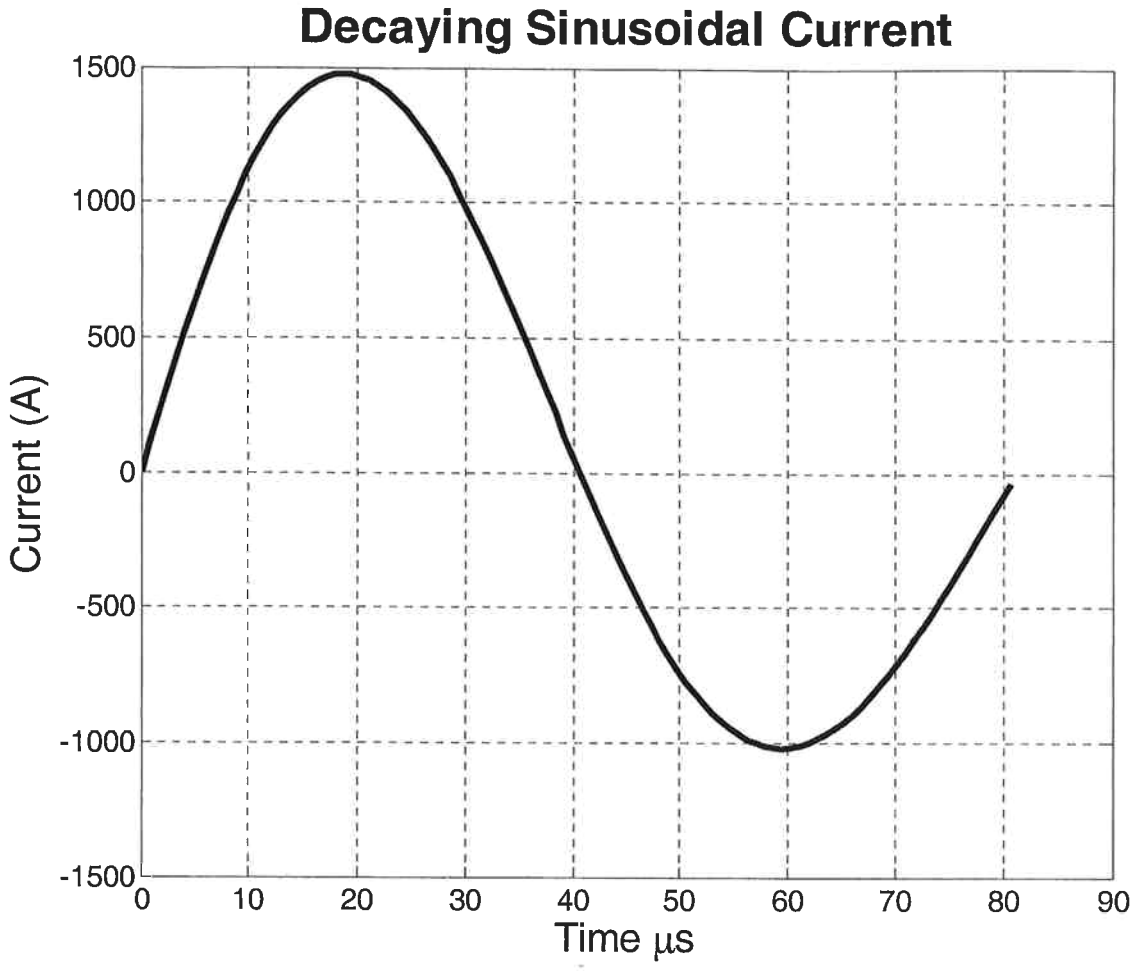

Fig. 2 Characteristic transcranial magnetic stimulation current.

Of particular interest is the time and value of the current peak,

$$t_p = \frac{\tan^{-1}\left(\frac{\omega}{\alpha}\right)}{\omega} \tag{3}$$

$$I_p = V\ e^{-\left(\frac{\tan^{-1}\left(\frac{\omega}{\alpha}\right)}{\omega l\,\alpha}\right)}\sqrt{\frac{C}{L}} \tag{4}$$

Neural Response

Motor and sensory thresholds for time varying magnetic fields are related to the rheobase and chronaxie strength through strength duration curves. For magnetic stimulation Geddes reports the rheobase and chronaxie results summarized in Table I [6].

Table I Neural magnetic stimulation response parameters

	Strength Duration Curve Parameters			
	Rheobase (β)		Chronaxie (γ)	
	Median (V/m)	Std. Dev. (V/m)	Mean (μs)	Std. Dev. (μs)
Sensory	6.75	2.06	329	78.4
Motor	16	6.1	203	78.5

Duration was defined as "onset to zero", or one-half cycle. In terms of the stimulus frequency f, and the table parameters β and γ, the electric field is

$$E = \beta \cdot (1 + 2\gamma f) \tag{5}$$

Fig. 3 shows the required induced electric field as a function of frequency.

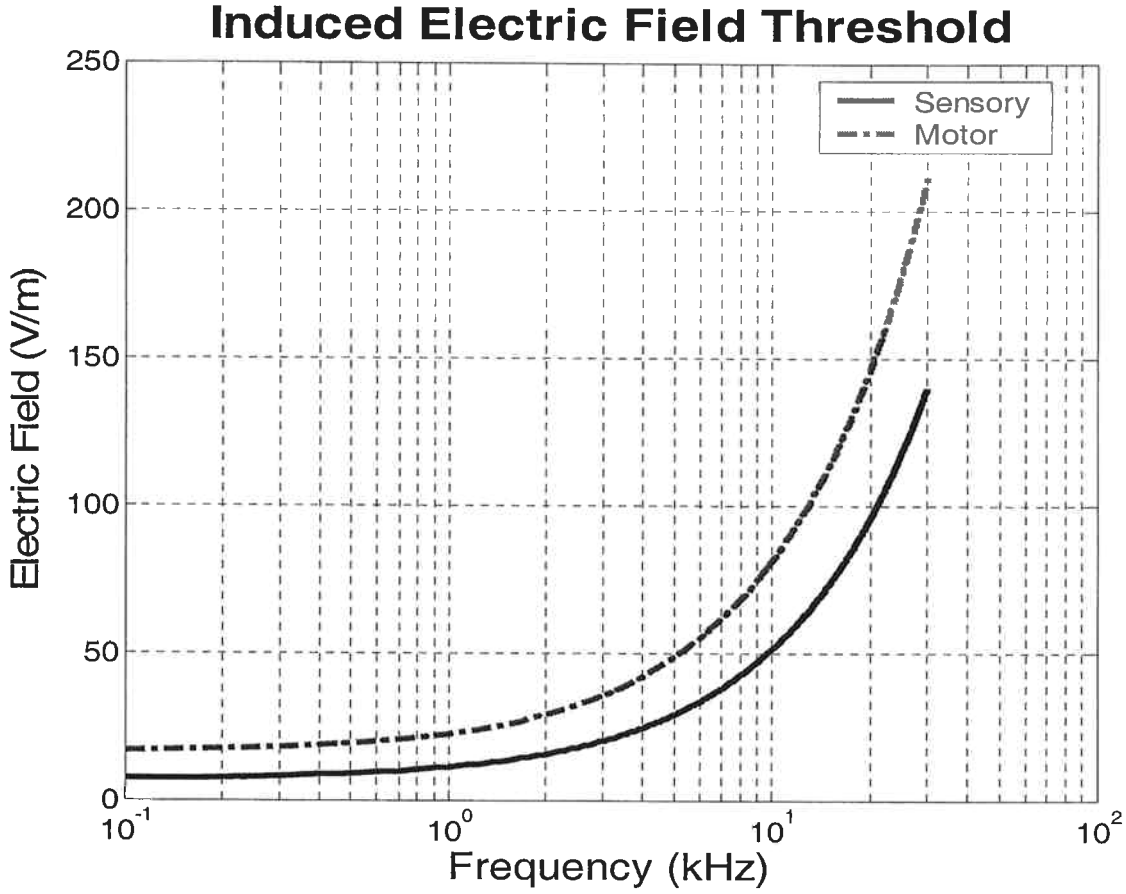

Fig. 3 Neural Stimulation threshold as a function of frequency.

Optimization

Consider the simple air core stimulator shown in Fig. 4. One quarter of the problem is displayed. The "C" shaped block can be considered the mandrel for the coil. This shape is chosen because it will be treated as a shell for the first part of the analysis, and then filled with steel using a tape wound core for the second part. A typical induced electric field pattern is shown in Fig. 5. The peak field occurs along the center axis of the core.

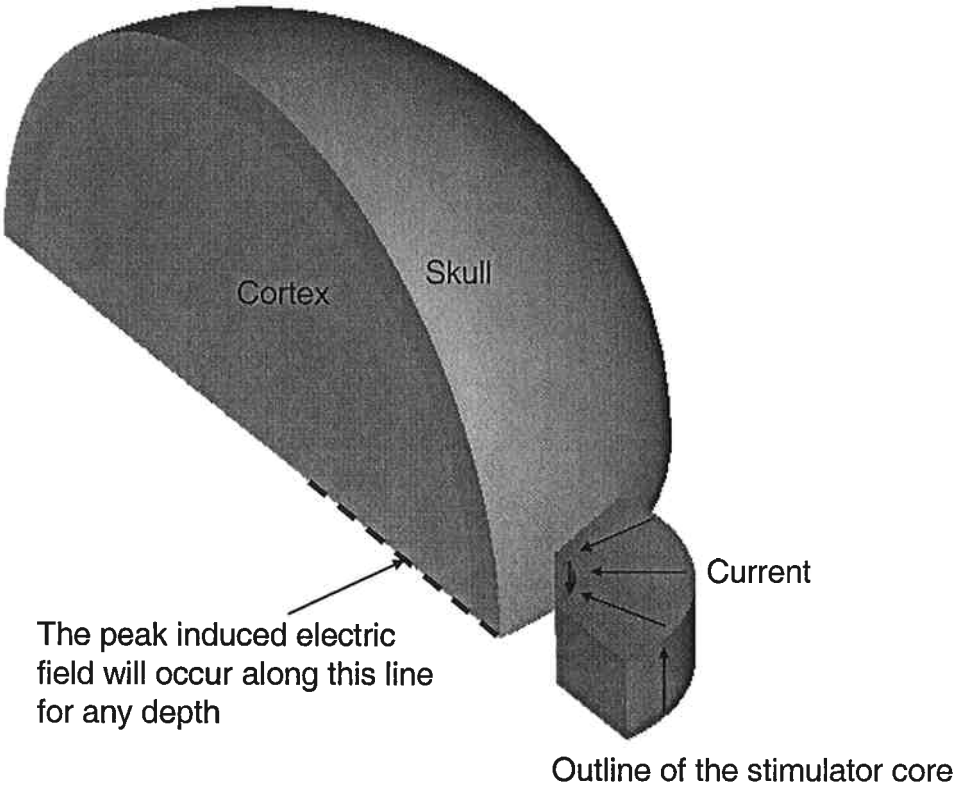

Fig. 4 Stimulator core next to the brain in quarter plane perspective.

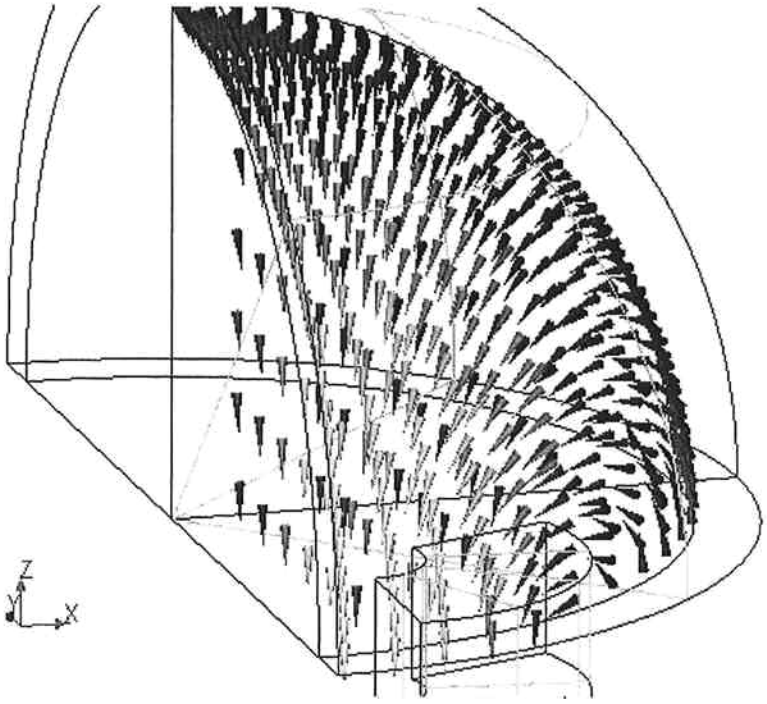

Fig. 5 Induced electric field arrow plot.

What constitutes an optimized system? Among the items that might be optimized are the following:

- Capacitor Size
- Core Stimulator Size
- Voltage
- Energy

Energy involves both the capacitor and the voltage. The number of turns N increases the resistance, and lowers the peak current in (4).

Air Core

An air core optimization is simplest. Many finite element and boundary element programs are suitable for analyzing this type of problem. Since the air core represents a linear analysis, a three dimensional boundary element analysis [7] is employed to predict the electric field as a function of depth for various core sizes.

Analytic Optimization

Consider an air core in which energy is to be minimized, and the core shape is known. If the shape in Fig. 4 is known, then the problem can be solved using a numerical solver for the induced field E_0 at desired depth, at current I_0 and radian frequency ω_0. The actual induced electric field will scale from this value by the number of turns N, the actual peak current I_p and the frequency ω,

$$E = NE_0\left(\frac{I_p}{I_0}\right)\cdot\left(\frac{\omega}{\omega_0}\right) \tag{6}$$

The induced electric field is required to satisfy the requirement dictated in (5); this can be interpreted as a requirement on voltage V,

$$V = NI_0\left(\frac{\omega_0}{\omega}\right)\left(\frac{\beta(1+\gamma\omega/\pi)}{\mathrm{E}_0}\right)e^{-\left(\frac{\tan^{-1}\left(\frac{\omega}{\alpha}\right)}{\omega/\alpha}\right)}\sqrt{\frac{\mathrm{L}}{\mathrm{C}}} \tag{7}$$

Let L_0 represent the inductance of the core with 1 turn. The resistance is actually a bit complicated because it must account for that lost in the thyristor and the wire. As will be seen shortly, it must also account for the eddy and hysteresis loss in the core if it is magnetizable. For the moment consider only the loss from the wire, and consider the core to be filled with wire so that additional turns are added at the expense of a smaller cross-section. In this approximation, the inductance and resistance will scale as N^2,

$$\begin{aligned} L &= N^2 L_0 \\ R &= N^2 R_0 \end{aligned} \tag{8}$$

The energy can be written in terms of the two remaining unknowns C and N as

$$W = \frac{1}{2}L_0 I_0^{\,2}\left(\frac{\omega_0}{\omega}\right)^2\left(\frac{\beta(1+\gamma\omega/\pi)}{\mathrm{E}_0}\right)^2 e^{-2\left(\frac{\tan^{-1}\left(\frac{\omega}{\alpha}\right)}{\omega/\alpha}\right)} \tag{9}$$

Consider the one turn air core stimulator shown in Fig. 4. The inductance is 0.004 μH for an ID=3.214 cm, OD=10.66 cm, and height = 5.9 cm. The core induces an electric field of 4.273 mV/m with 1A of excitation with characteristic frequency 5.208 kHz. Using these parameters in (9) yields the energy requirement shown in Fig. 6 for a spread of capacitance values and number of turns. The equations clearly suggest the use of a small number of turns and a large capacitor. As will be seen shortly, when more realistic relationships are employed to relate resistance and inductance to the number of turns by incorporating parasitic lead inductance and resistance loss from the thyristor and core, this trend will change.

Numerical Optimization

When the problem is considered as a four parameter optimization in the variables C, V, N, and core size x it can no longer be solved analytically. A numerical approach allows the parameters such as resistance to be treated more realistically, with the inclusion of proper bounds on voltage. Assume the core size to be a scale parameter x, scaling all the dimensions equally from the core

origin. If ζ_0 represents the length of the core winding with one turn, then the length ζ of the winding with N turns, scaled by a value x is

$$\zeta = Nx\zeta_0 \tag{10}$$

The combined resistance of both the parasitic core resistance and the diode R_0 with one turn is about 20 mΩ. A reasonable approximation to the resistance to be used in (2) is

$$R = R_0\left(0.9 + 0.1\frac{\zeta}{\zeta_0}\right) \tag{11}$$

The leads have a parasitic inductance $L_{Parasitic}$ equal to about 3 μH. Allow the core to vary through a spread of sizes and compute the inductance as the flux linkage per amperage for each size $L_0(x)$. The inductance with N turns is

$$L = N^2 L_0(x) + L_{Parasitic} \tag{12}$$

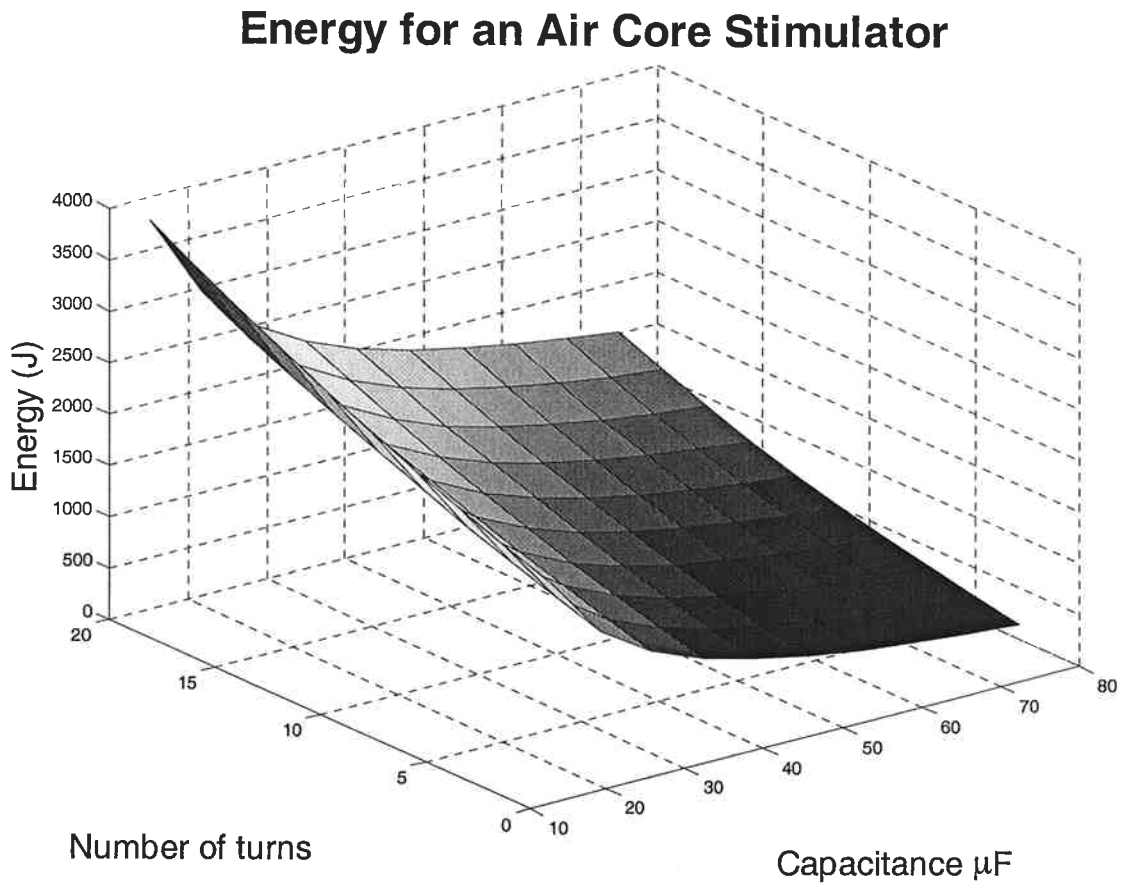

Fig. 6 Energy required for stimulation at a depth of 1 cm for a spread of capacitance and turns options.

Compute the induced electric field $E_0(x)$ with a current of I_0 A at radian frequency ω_0 for a spread of stimulation depths. Equation (6) dictates the induced electric field as delivered by the stimulator. If the inductance and induced electric field E_0 are fitted to the core size using a smooth spline, its derivative can be approximated and a variable metric procedure can be used to minimize an optimization index. If a combination of energy and stimulator core size are involved in the design objective, the optimization problem becomes

$$Min\ \ \Im = \frac{1}{2} CV^2 x$$

$$Subject\ \ to \tag{13}$$

$$NE_0 \left(\frac{I_p}{I_0} \right) \cdot \left(\frac{\omega}{\omega_0} \right) = \beta \left(1 + \frac{\gamma\omega}{\pi} \right)$$

I_p continues is determined from (4).

Optimization Algorithm

A word about the approach for this constrained optimization procedure is in order. Trust region algorithms are applicable, and the problem has strong local convergence. The basic idea is to approximate the problem to be minimized with a simpler function which reasonably reflects the behavior of real functional in a neighborhood near the solution sought [8]. This neighborhood is the trust region. Normally one step is taken to minimize the functional in question. A piecewise reflective search can be conducted at each iteration [9]. Sequential quadratic programming techniques have outperformed every other nonlinear optimization algorithm in terms of efficiency, accuracy, and percentage of successful solutions over a large range of test problems [10]. To quote the documentation from Matlab's algorithm documentation

> "Based on the work of Biggs [11], Han [12], and Powell ([13],[14]), the method allows you to closely mimic Newton's method for constrained optimization just as is done for unconstrained optimization. At each major iteration, an approximation is made of the Hessian of the Lagrangian function using a quasi-Newton updating method. This is then used to generate a QP subproblem whose solution is used to form a search direction for a line search procedure. An overview of SQP is found in Fletcher [15], Gill et al. [16], Powell [17], and Schittkowski [18]."

Results of the Air Core Numerical Optimization

Stimulation depth is a key parameter in the optimization. Fig. 7 shows how the system energy changes with target stimulation depth. Here a core shell with ID=1.836 cm, OD=6.096 cm, and height = 3.38 cm is scaled in all dimensions by a scale factor which varied from 1 to 1.75. The capacitance was allowed to vary from 5 to 75 μF, the voltage from 500 V to 3 kV, and the number of turns from 2 to 18. The problem has many local minima. A Monte Carlo method is employed to randomly vary the starting guess to increase the probability that the global minimum is found.

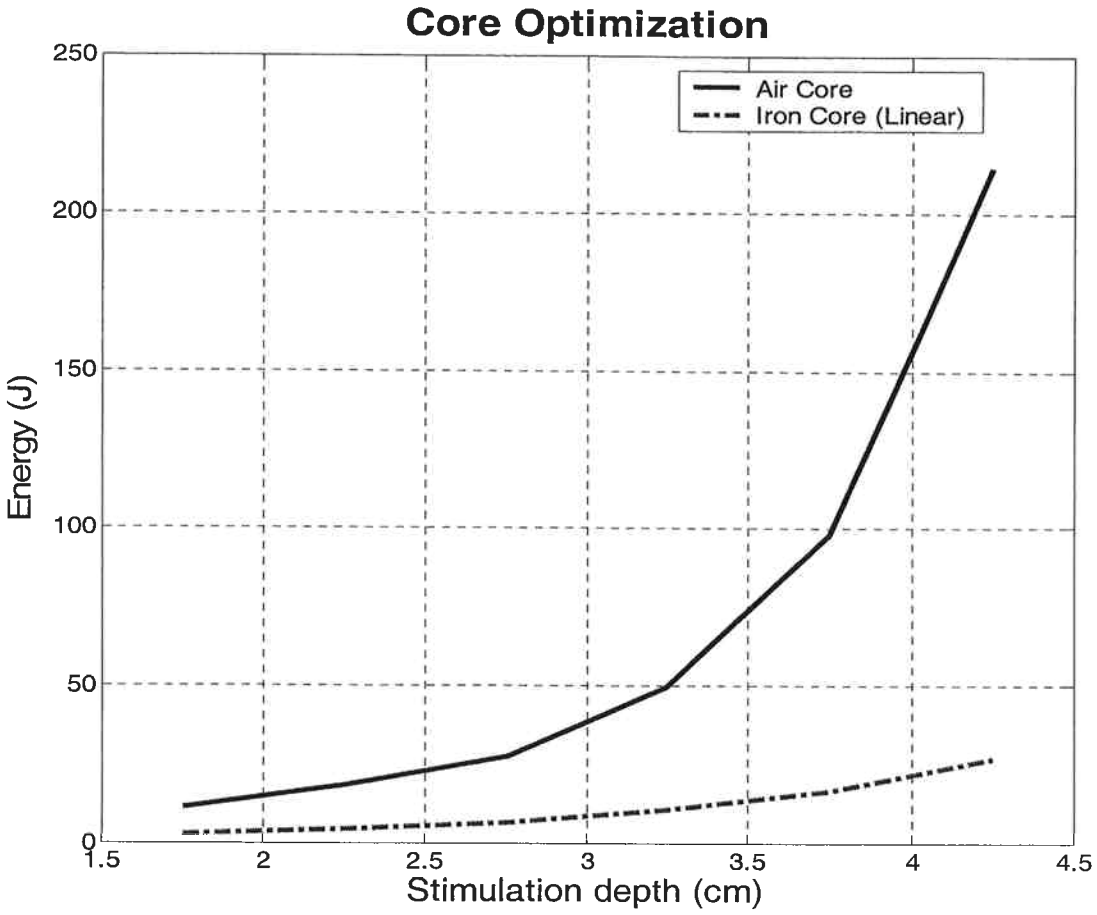

Fig. 7 Optimized energy as a function of various stimulation depths.

Table II shows the results of the optimization for each of the parameters. Among the key lessons are the following:

1. Smaller cores are desired for the lower stimulation depths.
2. Deeper stimulation target depths drive both the capacitance and the voltage up. The voltage comes up slower since it affects the optimization by its square.
3. When parasitic losses such as the switching and lead resistance are considered, the optimization always favors a higher number of turns. The neural response depicted in Fig. 3 is driving the frequency down with depth, and the inductance up.

Table II Optimization results for an air core stimulator.

Stimulation Depth (cm)	Scale Parameter	Capacitance (μF)	Voltage (kV)	Number of Turns	Frequency (kHz)	Stimulation Current (kA)
1.75	1.1621	5	2.1368	18	26.3319	30.6324
2.25	1.3918	5	2.6897	18	24.9194	36.3856
2.75	1.6752	6.1056	3	18	21.2232	41.8804
3.25	1.75	10.9834	3	18	15.5839	54.3823
3.75	1.75	21.7783	3	18	11.0567	74.5978
4.25	1.75	47.6275	3	18	7.4599	105.7719

Steel Core

Tape wound cores substantially reduce the required system size and energy requirements [19] [20], although their construction is more difficult [21]. The advantage is introduced with the price that the problem is nonlinear. The nonlinear element complicates the optimization in two respects. First, (2) no longer describes the current. The magnitude will be dictated by the degree of saturation. Second, the frequency is no longer a simple index. A core in saturation is characterized by a higher frequency and a lower amplitude. A fourier decomposition must be performed to determine the fundamental frequency amplitude and at least the first harmonic.

Linear

Much is to be learned by examining what should be expected from a steel core. The gap is very large. Treating the core as linear with a relative permeability of 1000 is a reasonable approximation. Fig. 7 shows how the energy drops with steel core in this approximation. Since the inductance is so high, the optimization parameters take a different posture. Important trends with iron cores are the following:

1. Deeper stimulation target depths require larger cores as with air cores.
2. Because of the high inductance, low capacitance is desirable.
3. As with air cores, voltage must increase with target stimulation depth.
4. Deeper target depths are commensurate with lower stimulation frequencies, and a lower frequency.
5. The required stimulation current increases nearly linearly with depth (4.25/1.75=2.43; 20.49/8.09=2.53). By contrast the required air core amp-turn excitation increases by 105.7/30.6=3.45. The iron core field does not fall off as rapidly with distance.

Table III Optimization parameters for a linear iron core stimulator using μ_r=1000.

Stimulation Depth (cm)	Scale Parameter	Capacitance (μF)	Voltage (kV)	Number of Turns	Frequency (kHz)	Stimulation Current (kA)
1.75	1.0022	5	1.0616	17.9702	13.7545	8.0951
2.25	1.2508	5	1.2975	15.2522	14.4552	8.8111
2.75	1.3283	5	1.6264	14.5454	14.4532	10.5291
3.25	1.3579	5	2.0476	14.334	14.4539	13.0631
3.75	1.3738	5	2.575	14.2388	14.4533	16.3166
4.25	1.3913	5.9533	3	13.7745	13.558	20.4981

Saturable Cores

The analysis becomes nonlinear with real magnetizable cores. The inductance of the core is computed using a numerical analysis routine for a spread of excitation current.
The equations governing the current in the RLC circuit are

$$\frac{d\lambda}{dt} + RI + \frac{1}{C}\int I\,dt = 0 \tag{14}$$

where the core flux linkage $\lambda = L \cdot I$, and L is a function of current I. To determine L(I), the core is excited through a spread of current, and the flux computed for each excitation. The governing equation is

$$\left(L + I\frac{dL}{dI}\right)\frac{d^2I}{dt^2} + \left(2\frac{dL}{dt} + I\frac{d^2L}{dI^2}\right)\left(\frac{dI}{dt}\right)^2 + R\frac{dI}{dt} + \frac{I}{C} = 0 \tag{15}$$

The flux has two components of change, one due to the changing current, and the second due to the changing inductance. A Runge Kutta Fehlberg technique based on the Dormand Prince pair [22] [23] was employed to integrate this equation numerically. Assume a scale parameter of 1.25, capacitance of 15 μF, a 12 turn coil. The current for the nonlinear core is shown in Fig. 8. As anticipated by (2), the time period has dropped, consistent with the lower inductance during excitation. Second, and more importantly, shoulders appear on the current waveform, and the current increases dramatically at mid point. This distorted waveform with higher current is the earmark of a core in saturation. The linear core current shown dashed has a larger inductance and a longer time period. The inductance follows the profile in the lower trace in Fig. 8.

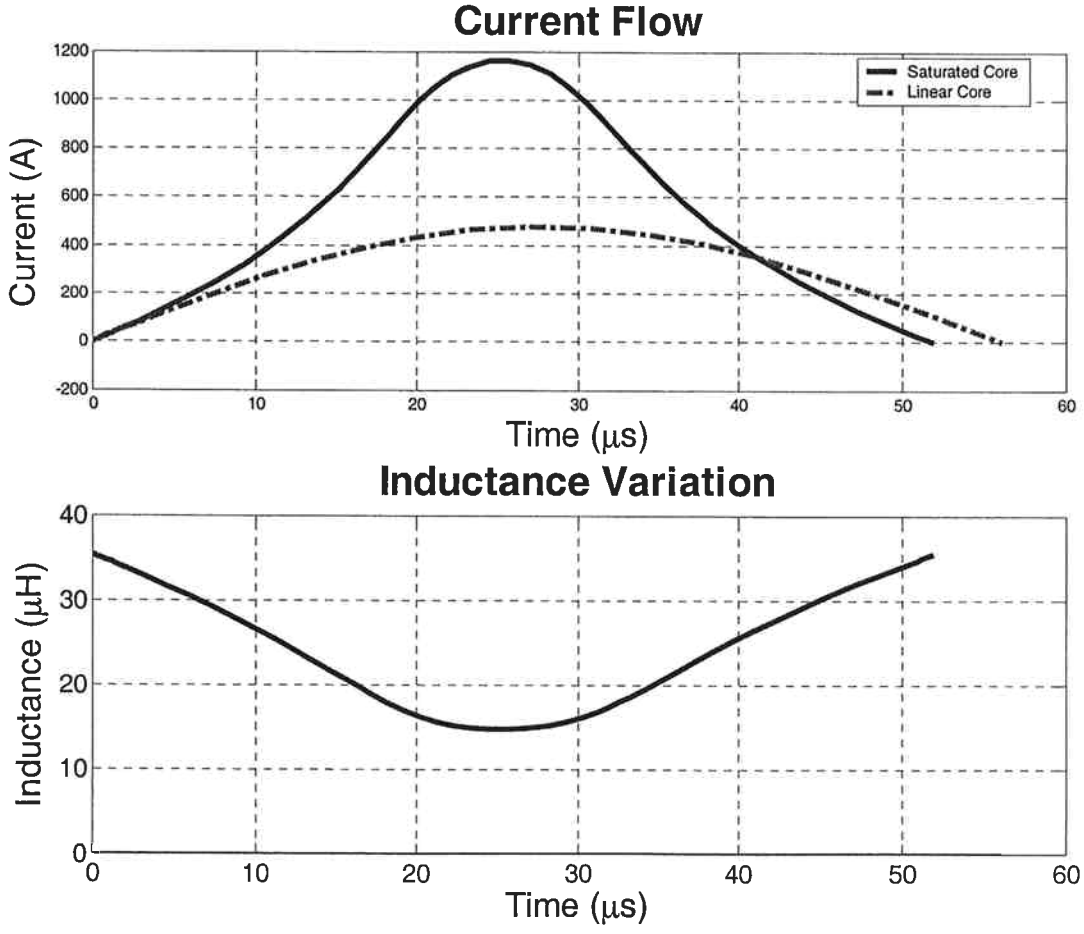

Fig. 8 Current and inductance as a function of time for a nonlinear core.

A least square curve fit routine is used to determine the fundamental component of the peak current and the frequency ω. Since the electric field is computed a priori for a range of current at a fixed frequency ω_0, a spline is used correlate the circuit delivered amp-turn peak with the field theory computed E field. As far as the field analysis program is concerned, the core is excited at the fundamental amplitude. The numerical field analysis is solved only at frequency ω_0. This E field must be scaled by the ratio of the circuit frequency as dictated by the zero crossing to the field analysis frequency, ω/ω_0. Table IV shows the results of the nonlinear analysis allowing the capacitance to vary from 5 to 35 μF, the number of turn from 1 to 18, the voltage from 400 V to 1.5 kV, and the core scale parameter from 1 to 1.75, using a parasitic inductance of 4.5 μH..

Table IV Results for a nonlinear core analysis

Target Depth (cm)	Scale Parameter	Capacitance (μF)	Voltage (kV)	Number of Turns	Frequency (kHz)	Stimulation Current (kA)	Energy (J)
1.75	1.7167	15.8764	0.4206	13.655	6.2797	1.4495	1.4041
2.25	1.75	35	0.4	13.984	4.0998	2.0442	2.8002
2.75	1.5021	34.9972	0.4002	18	3.54	2.3122	2.8027
3.25	1.75	34.9537	0.5752	18	3.2554	3.3454	5.7818
3.75	1.75	34.9579	0.6896	18	3.2552	4.0112	8.3118
4.25	1.75	34.9994	0.8136	18	3.2533	4.7351	11.583

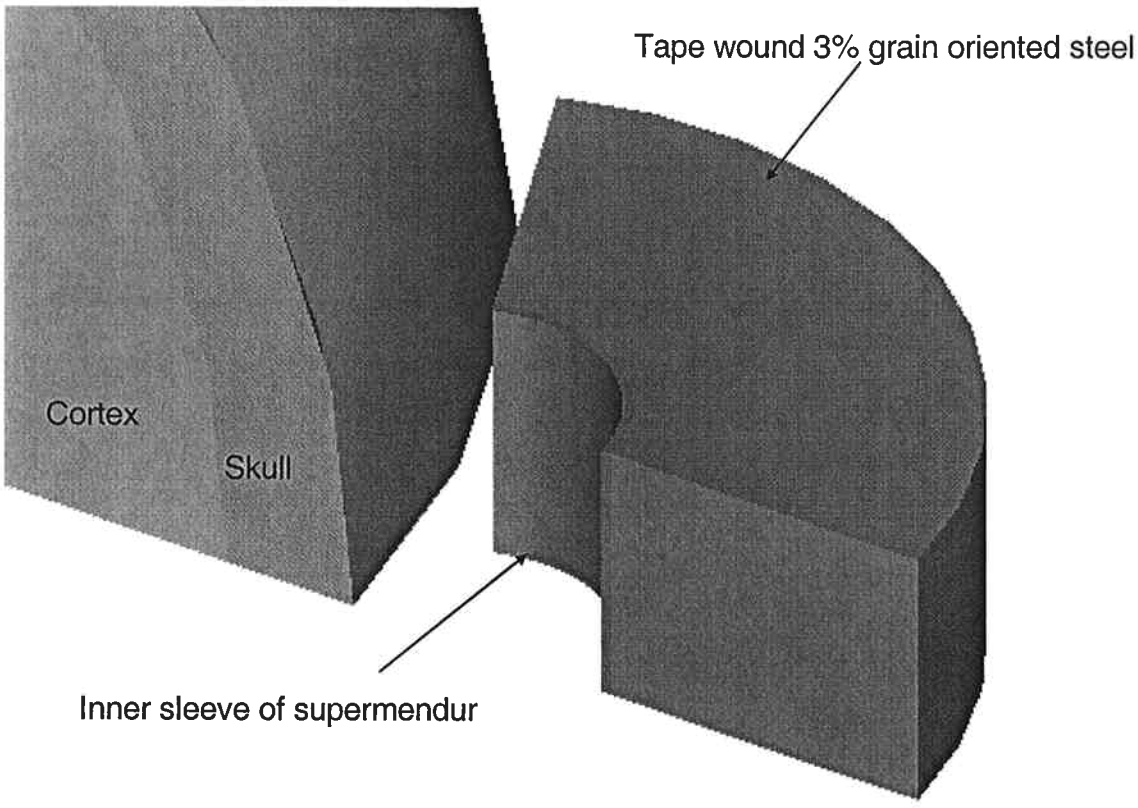

Fig. 9 Mixed saturable core with supermendur on the inner region.

Consider a mixed core with the inside region composed of tape wound supermendur Hyperco) rather than tape wound M-19 such as that shown in Fig. 9. If the inner region comprises 2.2 % of the core, the optimized parameter table changes to Table V. This exchange is questionable since the cost of even a very small piece slice of supermendur is very high.
Experiments indicate the energy required to achieve motor threshold in the cortex is higher than that reported in Table IV and Table V, closer to 10-15 J, and the stimulation site is thought to be about 3 cm deep. This energy increases with parasitic inductance and resistance. The parasitic inductance 4.5 H might be low. The results in Table I are for peripheral nerves; cortex stimulation is probably higher. This team is not aware of similar data for the cortex. Barker [24] presented stimulation results for energy and frequency without reference to the electric field.

Table V Mixed stimulation core with 2.2% of the inner region exchanged for supermendur.

Target Depth (cm)	Scale Parameter	Capacitance (μF)	Voltage (kV)	Number of Turns	Frequency (kHz)	Stimulation Current (kA)	Energy (J)
1.75	1.75	5	0.5778	17.443	8.7792	1.2867	0.8347
2.25	1.75	8.8148	0.5791	18	6.4206	1.7299	1.4779
2.75	1.7499	34.9437	0.4656	18	3.2241	2.7102	3.788
3.25	1.7462	34.0444	0.5703	18	3.2689	3.2787	5.5369
3.75	1.7498	34.1008	0.6823	18	3.2638	3.9256	7.9376
4.25	1.75	32.942	0.8123	18	3.3206	4.5969	10.868

Conclusions

A method is presented for optimizing a magnetic stimulation system. The frequency, system voltage, capacitance, core stimulator size, and the number of turns are treated as unknowns. Based on the neural magnetic stimulation response parameters, and the electric field as computed through a boundary element solver, the ideal parameters for the system can be derived. A trust region technique is used to solve the four parameter optimization problem. The result is target depth dependent. Deeper targets are commensurate with lower excitation stimuli, and higher amp-turn products.

Acknowledgment

This research was supported by Neuronetics, Inc.

References

[1] K. Hsu, S. Nagarajan, and D. Durand, "Analysis and efficiency of Magnetic Stimulation", *IEEE Trans. Bio.* Engr., Vol. 50, No. 11, November 2003, pp. 1276-1285.
[2] P. Ravazzani, G. Tognola, J. Ruohenen, and F. Grandori, "Frequency related effects and geometrical characteristics", *Proc. 22nd Annual EMBS Int. Conference*, Chicago, IL, July 23-28, 2000, pp. 2625-2628.
[3] T. Onuki, S. Wakao, T. Miyokawa, and Y. Nishimura, "Design Optimization of Simulation Coil System for Nerve Stimulation", *IEEE Trans. Magn.*, vol. 34, no. 4, July 1998, pp. 2159-2161.
[4] K. H. Hsu and D. Durand, "A 3D differential coil design for localizing magnetic stimulation", *IEEE Trans. Biomed. Engr.*, vol. 48, Oct 2001, pp. 1162-1168.
[5] N. Al-Mutawaly and Raymond Findlay, " A Novel coil design for magnetic nerve stimulation", *IEEE Canadian Conference on Electrical and Computer Engineering*, Vol. 2 , 24-28 May 1998, pp. 669 – 672.

[6] J.D. Bourland, J.A. Nyenhuis, W.A. Noe, J.D. Schaefer, K.S. Foster, and L.A. Geddes, "Motor and Sensory Strength-duration Curves for MRI Gradient Fields," Proceedings of the International Society of Magnetic Resonance in Medicine 4th Scientific Meeting and Exhibit, New York, NY, 1996, p. 1724.

[7] Dalian Zheng, "Three dimensional eddy current analysis by the boundary element method", *IEEE Trans. Magn.* Vol. 33, no. 2, March 1997, pp. 1354-1357.

[8] Moré, J.J. and D.C. Sorensen, "Computing a Trust Region Step," *SIAM Journal on Scientific and Statistical Computing*, Vol. 3, pp 553-572, 1983.

[9] Coleman, T.F. and Y. Li, "A Reflective Newton Method for Minimizing a Quadratic Function Subject to Bounds on some of the Variables," *SIAM Journal on Optimization*, Vol. 6, Number 4, pp 1040-1058, 1996.

[10] Schittkowski, K., "NLQPL: A FORTRAN-Subroutine Solving Constrained Nonlinear Programming Problems," Annals of Operations Research, Vol. 5, pp 485-500, 1985.

[11] Biggs, M.C., "Constrained Minimization Using Recursive Quadratic Programming," Towards Global Optimization (L.C.W. Dixon and G.P. Szergo, eds.), North-Holland, pp 341-349, 1975.

[12] Han, S.P., "A Globally Convergent Method for Nonlinear Programming," *J. Optimization Theory and Applications*, Vol. 22, p. 297, 1977.

[13] Powell, M.J.D., "The Convergence of Variable Metric Methods for Nonlinearly Constrained Optimization Calculations," Nonlinear Programming 3, (O.L. Mangasarian, R.R. Meyer and S.M. Robinson, eds.), Academic Press, 1978.

[14] Powell, M.J.D., "A Fast Algorithm for Nonlinearly Constrained Optimization Calculations," Numerical Analysis, G.A.Watson ed., Lecture Notes in Mathematics, Springer Verlag, Vol. 630, 1978.

[15] R., "Practical Methods of Optimization," Vol. 1, Unconstrained Optimization, and Vol. 2, Constrained Optimization, John Wiley and Sons, 1980.

[16] Gill, P.E., W. Murray, and M.H.Wright, Practical Optimization, London, Academic Press, 1981.

[17] Powell, M.J.D., "Variable Metric Methods for Constrained Optimization," Mathematical Programming: The State of the Art, (A. Bachem, M. Grotschel and B. Korte, eds.) Springer Verlag, pp 288-311, 1983.

[18] Hock, W. and K. Schittkowski, "A Comparative Performance Evaluation of 27 Nonlinear Programming Codes," *Computing*, Vol. 30, p. 335, 1983.

[19] K. R. Davey, C. H. Cheng, and C. M. Epstein, "An alloy – CORE electromagnet for transcranial brain stimulation," *Journal on Clinical Neurophysiology*, vol. 6, no. 4, pg. 365, 1989.

[20] C.M. Epstein and K.R. Davey, "Iron-core coils for transcranial magnetic stimulation," *Journal of Clinical Neurophysiology*, vol. 19, no. 4, pp. 376-381, December, 2002.

[21] K. Davey and C.M. Epstein, "Magnetic stimulation coil and circuit design," *IEEE Transactions on Biomedical Engineering*, vol. 47, no. 11, pp. 1493-1499, November, 2000.

[22] Forsythe, G. , M. Malcolm, and C. Moler, Computer Methods for Mathematical Computations, Prentice-Hall, New Jersey, 1977.

[23] Kahaner, D. , C. Moler, and S. Nash, Numerical Methods and Software, Prentice-Hall, New Jersey, 1989.

[24] A. Barker, C. Garnham, and I. Freeston, "Magnetic nerve stimulation: the effect of waveform on efficiency, determination of neural membrane time constants, and the measurement of stimulator output", Magnetic Nerve Stimulation: Basic Principles of Clinical Experience, ed. W.J. Levy, R.O. Cracco, A.T. Barker, and J. Rothwell, Elsevier Science Publishers, EEG Supplemental 43, 1991, pp. 227-237.